PNAS INAUGURAL ARTICLE | NEUROSCIENCE

An excitatory peri-tegmental reticular nucleus circuit for wake maintenance

John M. Webb[a,b,c], Mingyang Ma[a], Chen Yin[a,b,c], Louis J. Ptáček[a,b,c,d,1], and Ying-Hui Fu[a,b,c,d,1]

This contribution is part of the special series of Inaugural Articles by members of the National Academy of Sciences elected in 2018.

Contributed by Ying-Hui Fu; received February 22, 2022; accepted June 24, 2022; reviewed by Patrick M. Fuller and Zhi-Li Huang

Sleep is a necessity for our survival, but its regulation remains incompletely understood. Here, we used a human sleep duration gene to identify a population of cells in the peri-tegmental reticular nucleus (pTRN^{ADRB1}) that regulate sleep–wake, uncovering a role for a poorly understood brain area. Although initial ablation in mice led to increased wakefulness, further validation revealed that pTRN^{ADRB1} neuron stimulation strongly promotes wakefulness, even after stimulation offset. Using combinatorial genetics, we found that excitatory pTRN^{ADRB1} neurons promote wakefulness. pTRN neurons can be characterized as anterior- or posterior-projecting neurons based on multiplexed analysis of projections by sequencing (MAPseq) analysis. Finally, we found that pTRN^{ADRB1} neurons promote wakefulness, in part, through projections to the lateral hypothalamus. Thus, human genetic information from a human sleep trait allowed us to identify a role for the pTRN in sleep–wake regulation.

sleep | FNSS | wake | pTRN | short sleep

Many animals spend more time sleeping than engaging in any other single behavior (1). Although sleep is a time-consuming activity, sleep is vital for normal organismal function and survival (2). Poor sleep can lead to increased risk for a wide variety of diseases and health conditions, but a full accounting of the brain regions and cell types regulating sleep duration remains lacking (2).

A wide variety of techniques have been used to reveal regions regulating sleep. Seminal lesion studies in cats; immediate early gene markers during sleep deprivation; tracking developmental cell lineage; insights from human disease affecting sleep; and tracing from known sleep regions have played a role in uncovering new cell types and regions (3–14). Insights from genetics have also played a role in discovering new cell types, perhaps most notably hypocretin (HCRT, also known as orexin) that subsequently led to the discovery of hypothalamic HCRT–expressing neurons, which serve as a druggable target for the treatment of sleep disorders in humans (15–17). We also sought to use genetics to uncover sleep-regulating regions. Recently, several genes were implicated in causing familial natural short sleep (FNSS) in humans, and mice with these point mutations also sleep less (18–21). We took advantage of one of these known human FNSS sleep genes, beta-1 adrenoreceptor (*ADRB1*) (18), to help guide the search for novel brain regions involved in sleep regulation. Although we previously showed that ADRB1-postitive neurons participate in sleep regulation in the dorsal pons (DP), we studied the dorsal pontine region simply based on the high expression level of *ADRB1* in this region (18). This does not exclude the possibility of an additional important region(s) for sleep regulation through ADRB1 neurons. To investigate the possibility that other ADRB1 neurons regulate sleep, we ablated ADRB1 neurons in many brain regions in an unbiased manner. To increase experimental throughput of screening of regions, we initially relied on video tracking to measure time of inactivity as a proxy for sleep, which decreased the amount of analysis time compared with manually scoring electroencephalogram/electromyography (EEG/EMG).

Through our screening experiment, we identified ADRB1 neurons in and around the tegmental reticular nucleus (TRN) as a group of neurons regulating sleep duration. We refer to the TRN and surrounding region as the peri-TRN (pTRN). The pTRN is dorsal to the middle cerebellar peduncle and encompasses the TRN and the ventral aspect of the median raphe nuclei. The pTRN is a poorly described brain region in the ventral pons that is thought to be involved in saccadic eye movements (22). We subsequently investigated the natural activity of pTRN^{ADRB1} neurons during sleep–wake states, measured the effects of acute and chronic manipulations of pTRN^{ADRB1} neurons on the sleep–wake state, and used combinatorial genetics and projection patterns to elucidate pTRN^{ADRB1} neuron subtypes important for regulating sleep. Together, our

Significance

Although many brain regions have been shown to participate in sleep–wake regulation using model organisms, we sought to identify a region relevant to human sleep duration regulation. We started from a human sleep duration gene (*ADRB1*) and then used an unbiased approach to identify the peri-tegmental reticular nucleus (pTRN^{ADRB1}) as a region participating in sleep–wake regulation. We found that pTRN^{ADRB1} neurons are wake-active and are potent promoters of wakefulness, with their activation promoting wakefulness well after the end of stimulation. Further, combinatorial genetics revealed that excitatory pTRN^{ADRB1} neurons are primarily responsible for this phenotype and that they act in part through projections to the lateral hypothalamus. Thus, the pTRN plays an important role in sleep–wake regulation.

Author contributions: J.M.W. and Y.-H.F. designed research; J.M.W., M.M., and C.Y. performed research; J.M.W. and M.M. contributed new reagents/analytic tools; J.M.W., M.M., and C.Y. analyzed data; J.M.W., L.J.P., and Y.-H.F. wrote the paper; and L.J.P. helped revise the paper.

Reviewers: P.M.F., University of California; and Z.-L.H., Fudan University.

The authors declare no competing interest.

[1]To whom correspondence may be addressed. Email: Louis.Ptacek@ucsf.edu or Ying-Hui.fu@ucsf.edu.

This article contains supporting information online at http://www.pnas.org/lookup/suppl/doi:10.1073/pnas.2203266119/-/DCSupplemental.

Published July 28, 2021.

results establish a crucial role for pTRN^{ADRB1} neurons in sleep regulation and highlight the value of genetic analyses of human sleep variants to guide the search for novel sleep regions.

Results

pTRN^{ADRB1} Neurons Regulate Wake Duration. In order to identify brain regions important for human sleep regulation, we took advantage of the *ADRB1* mutation shown to cause FNSS in humans. We hypothesized that some ADRB1-positive neurons should be important for regulating sleep–wake duration and that crucial neurons for sleep–wake duration should show a phenotype when ablated. We began by injecting 100 to 300 nL of caspase virus (AAV1.hSyn.Flex.taCasp3), which should ablate Cre-positive neurons, into eight brain areas in either ADRB1-Cre mice or their wild-type (WT) littermate controls and measured mobile time over a 24-h period using video tracking (Fig. 1*A*). We found that pTRN-injected ADRB1-Cre mice had ∼3 h more mobile time than WT controls, while injections of seven other regions resulted in no significant changes (Fig. 1*A*). This increase in mobile time was due to an increase in mobile time during the dark period (*SI Appendix*, Fig. S1). Our ADRB1-Cre line labels a population of cells in the ventral pons roughly outlined by the pTRN that is just above the middle cerebellar peduncle (Fig. 1*B*).

To confirm the results from our screening experiment and to measure the effect of ablating pTRN^{ADRB1} neurons on sleep–wake substates, we repeated the caspase-mediated ablation in a new cohort of mice and simultaneously measured sleep state with EEG/EMG (Fig. 1*C*). We found that ablating pTRN^{ADRB1} neurons led to an increase in total wake time of ∼3 h with corresponding decreases in both rapid eye movement (REM) and nonrapid eye movement (NREM) sleep, an effect that was mostly limited to the dark period (Fig. 1 *D* and *E*). However, recovery sleep after sleep deprivation was unaffected (*SI Appendix*, Fig. S2). A decrease in pTRN^{ADRB1} neuron number was confirmed by measuring ADRB1-expressing cells in the pTRN (Fig. 1 *F*–*H*).

This 3-h increase in wake time in pTRN^{ADRB1}-ablated mice can be explained by an increase in wake-to-wake epoch transition probability and a decrease in wake-to-NREM epoch transition probability (Fig. 1*I*). Indeed, pTRN^{ADRB1}-ablated mice showed a decrease in both wake and NREM bout number but an increase in wake bout length (Fig. 1 *J* and *K*). Furthermore, to confirm that localized chronic silencing of pTRN^{ADRB1} neurons affected sleep time, we silenced pTRN^{ADRB1} neurons by tetanus neurotoxin (TeNT), which can block calcium-evoked presynaptic vesicle fusion and transmitter release. We found that even a small injection volume (50 nL) of TeNT virus (AAV-DJ.CMV.DIO.eGFP.2A.TeNT) was sufficient to increase total wake time (*SI Appendix*, Fig. S3). Together, these results confirmed that pTRN^{ADRB1} neurons are important for regulating sleep duration.

Endogenous Activity of pTRN Neurons. After establishing that chronic silencing or ablation of pTRN^{ADRB1} neurons increased wake duration, we next sought to establish the endogenous role of pTRN^{ADRB1} neurons in sleep–wake behavior. Since the

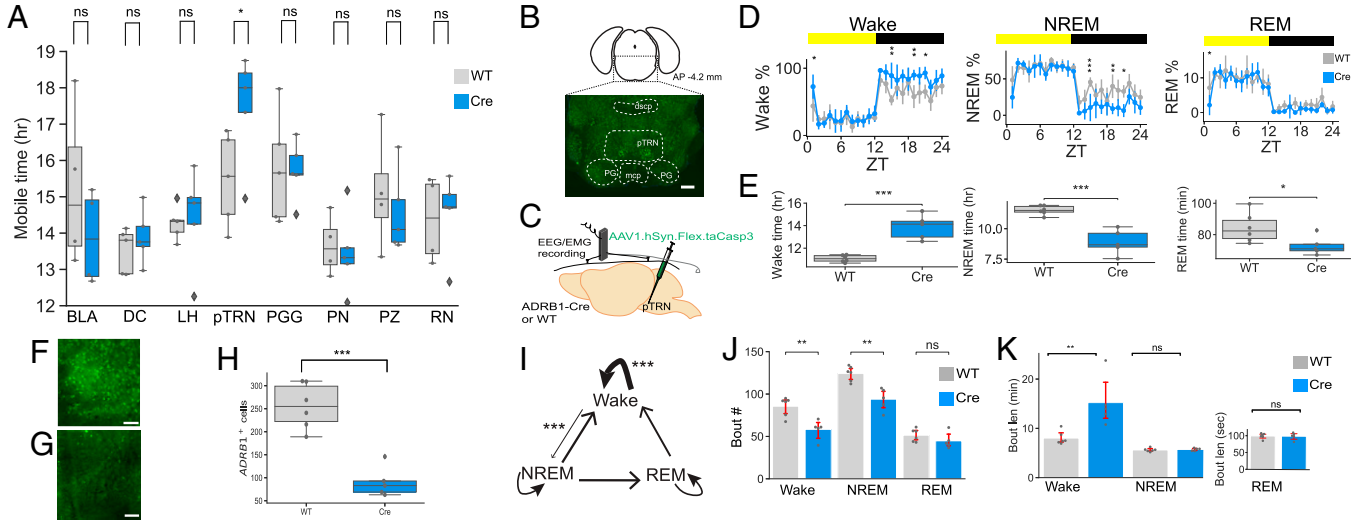

Fig. 1. Discovery of the pTRN region in sleep–wake regulation. (*A*) Total mobile time averaged over 4 consecutive days with video tracking for ADRB1-Cre (n = 4 to 5) and WT (n = 4 to 5) littermate mice injected with AAV1.hSyn.Flex.taCasp3.TEVp into the indicated regions. (WT vs. Cre, P = 0.0225, random sampling with replacement bootstrap, 10,000 iterations, ns $P > 0.05$, *$P < 0.05$). See also *SI Appendix*, Fig. S1. (*B*) Schematic showing the coronal location of the pTRN. The *Inset* shows pTRN^{ADRB1} neurons from an ADRB1-Cre mouse crossed to an L10a reporter. (Scale bar, 400 μm.) (*C*) Experimental schematic for caspase ablation combined with EEG/EMG recording. (*D*) Hour-by-hour quantification of wake (*Left*), NREM (*Middle*), or REM (*Right*) over a 24-h period from ADRB1-Cre (n = 5) or WT littermate (n = 6) mice averaged over 2 consecutive days. The lights-on period (12 h) is denoted by a yellow bar, while the lights-off period is denoted by a black bar. (WT vs. Cre, two-way RM ANOVA with post hoc Sidak's multiple comparisons test, *$P < 0.05$, **$P < 0.01$, ***$P < 0.001$). See also *SI Appendix*, Fig. S3. (*E*) Total time spent in wake (*Left*), NREM (*Middle*), or REM (*Right*) from *D*. (WT vs. Cre, wake: P = 0.0002, NREM: P = 0.0002, REM: P = 0.044, Student's two-sided t test, *$P < 0.05$, ***$P < 0.001$). (*F* and *G*) Representative in situ staining from a caspase-injected WT (*F*) or ADRB1-Cre (*G*) mouse. (Scale bar, 60 μm.) (*H*) Quantification of cells positive for *Adrb1* using in situ staining from ADRB1-Cre (n = 5) or WT littermate (n = 6) mice from *D* (WT vs. Cre, P = 0.0001, Student's two-sided t test, ***$P < 0.001$). (*I*) Quantification of sleep–wake epoch transition changes from ADRB1-Cre (n = 5) or WT littermate (n = 6) mice. There was an increase in wake-to-wake epoch transition probability and a decrease in wake-to-NREM epoch transition probability for ADRB1-Cre vs. WT mice. Thicker lines imply increases in state change, while thinner lines imply decreases in state change in ablated mice (WT vs. Cre, wake-to-wake transition: P = 0.0006, wake-to-NREM transition: P = 0.0006, Student's two-sided t test, ***$P < 0.001$). (*J*) Quantification of wake, NREM, and REM bout number from *D* (WT vs. Cre, wake: P = 0.0032, NREM: P = 0.0013, REM: P = 0.2214, Student's two-sided t test, ns $P > 0.05$, **$P < 0.01$). (*K*) Quantification of wake, NREM, and REM bout length from *D* (WT vs. Cre, wake: P = 0.0076, NREM: P = 0.627, REM: P = 0.9816, Student's two-sided t test, ns $P > 0.05$, **$P < 0.01$). BLA, basolateral amygdala; DC, dorsal cochlea; dscp, superior cerebellar peduncle decussation; LH, lateral hypothalamus; mcp, middle cerebellar peduncle; pTRN, peri-tegmental reticular nucleus; PG, pontine gray; PGG, paragigantocellular nucleus; PN, pedunculopontine nucleus; PZ, parafacial nucleus; RN, nucleus of reunions. Error bars represent ± SEM for *D*, *J*, and *K*. For *A*, *E*, and *H*, the boxes show the quartiles, and the whiskers show the rest of the distribution.

endogenous firing rate of pTRN neurons had not been established, we began by applying in vivo electrophysiology with a 32-channel probe to determine the firing rate of pTRN neurons (Fig. 2 *A*–*C*). We found that the firing rate of pTRN neurons ranged between 4 and 21 Hz (*SI Appendix*, Fig. S4). We also found that the firing rate of pTRN neurons was highest during wakefulness and lowest during REM, with an intermediate firing rate during NREM, though there was a mixture of some neurons that had higher firing rates in REM compared with NREM (Fig. 2 *D* and *E*).

We then performed bulk calcium imaging to specifically examine the activity of $pTRN^{ADRB1}$ neurons. We injected AAV1.Syn.Flex.GCaMP6s into the pTRN of ADRB1-Cre mice and measured changes in calcium fluorescence (ΔF/F, as an indicator of neuronal activity) while simultaneously measuring sleep–wake state by EEG/EMG (Fig. 2 *F* and *G*). We found that the ΔF/F of $pTRN^{ADRB1}$ neurons was highest during wake and REM, and lowest during NREM (Fig. 2*H*). The activity increased from NREM-to-wake and NREM-to-REM transitions and decreased from wake-to-NREM transitions (Fig. 2 *I* and *J*). For REM-to-wake transitions, there was an initial increase in activity followed by decreasing activity (Fig. 2 *I* and *J*).

Finally, to investigate the activity of $pTRN^{ADRB1}$ neurons on a single-cell level, we injected AAV1.Syn.Flex.jGCaMP7f combined with a gradient-index (GRIN) lens into the pTRN of ADRB1-Cre mice and measured ΔF/F with a miniscope (Fig. 2 *K* and *L*). We found that the ΔF/F of the majority of $pTRN^{ADRB1}$ neurons was higher during wake vs. NREM (Fig. 2*M*). Although some neurons had higher activity during NREM vs. REM, more than half had higher activity during REM compared with NREM (Fig. 2*M*). These results establish that $pTRN^{ADRB1}$ neurons are wake- and REM-active overall. However, at the single-cell level, most neurons were still predominantly wake-active, while REM activity was more heterogeneous (Fig. 2*M*).

Activation of $pTRN^{ADRB1}$ Neurons Promotes Wakefulness. Since $pTRN^{ADRB1}$ neurons are important for sleep duration regulation and are mostly wake- and REM-active, we hypothesized that we could alter the sleep–wake state by manipulating $pTRN^{ADRB1}$ neuron activity. We first used the designer receptors exclusively activated by designer drugs (DREADDs) method to activate $pTRN^{ADRB1}$ neurons on a longer timescale by injecting either Gq virus (AAV8.hSyn.DIO.hM3D(Gq).mCherry) or the control mCherry virus (AAV8.hSyn.DIO.mCherry) into the pTRN of ADRB1-Cre mice. The Gq virus allows $pTRN^{ADRB1}$ neurons to be activated by clozapine-n-oxide (CNO). We then administered either saline or CNO via intraperitoneal (IP) injection 3 wk after virus administration (Fig. 3*A*). We found that CNO injection at zeitgeber time (ZT) 1, a timepoint of high sleep pressure, increased wake for Gq-injected mice by more than 2 h in the 6-h postinjection period compared with either saline injection in Gq mice or CNO injection in mCherry mice, with corresponding decreases in both NREM and REM sleep (Fig. 3 *B* and *C*). Interestingly, injecting CNO at ZT12, a timepoint when the mice had low sleep pressure and were awake ∼80% even under saline-injected conditions, also produced significantly more wake in Gq mice vs. mCherry mice (*SI Appendix*, Fig. S5). In Gi-injected animals, CNO administration led to no change in sleep–wake state in the first 3 h after injection but an increase in wake in the following 3 h, possibly due to a rebound effect (*SI Appendix*, Fig. S6).

We next determined whether acute activation was sufficient to increase wakefulness using optogenetics (Fig. 3 *D* and *E*). We found that 10 or 20 Hz stimulation of $pTRN^{ADRB1}$ neurons was sufficient to immediately wake the mice up nearly 100% of the time, an effect not seen for the EYFP controls (Fig. 3 *F* and *G* and *SI Appendix*, Fig. S7). The increase in wakefulness continued well after the end of optogenetic stimulation as the mice remained awake at a higher percentage 2-3 min after the end of stimulation compared with 2-3 min before the simulation (Fig. 3 *F* and *H* and *SI Appendix*, Fig. S7). An analysis of trials that began with NREM or REM sleep at the start of the stimulation revealed that the stimulation could wake the mice from both NREM and REM sleep (*SI Appendix*, Fig. S7). Bilateral optogenetic inhibition of $pTRN^{ADRB1}$ neurons showed no effect on sleep–wake state (*SI Appendix*, Fig. S8). Taken together, these results indicate that acute or chronic activation of $pTRN^{ADRB1}$ neurons is sufficient to promote wakefulness, an effect that persists even after the end of stimulation.

$pTRN^{ADRB1;CaMKIIa}$ Neurons Promote Wakefulness. ADRB1 neurons can be either excitatory or inhibitory. Although our preliminary analysis suggested that the majority of $pTRN^{ADRB1}$ neurons express CaMKIIa (excitatory subtype), there were also some vesicular GABA transporter (VGAT)-positive (inhibitory subtype) $pTRN^{ADRB1}$ neurons. To determine the subtype of $pTRN^{ADRB1}$ neurons contributing to the wake-promoting phenotype, we used combinatorial genetics. To activate primarily excitatory $pTRN^{ADRB1}$ neurons, we injected both AAV9.CaMKIIa.EGFP.T2A.FLPo and AAV9.hSyn.Con/Fon.hChR2(H134R).EYFP into the pTRN of ADRB1-Cre mice (Fig. 4*A*) to restrict the expression of ChR2 to $pTRN^{ADRB1;CaMKIIa}$ neurons. We then stimulated these $pTRN^{ADRB1;CaMKIIa}$ neurons at either 10 or 20 Hz and observed that both stimulation frequencies were sufficient to promote wakefulness (Fig. 4*B* and *SI Appendix*, Fig. S9). Similar to activating all $pTRN^{ADRB1}$ neurons, stimulating $pTRN^{ADRB1/CaMKIIa}$ neurons was sufficient to increase wakefulness 2-3 min after light activation (Fig. 4*C*). To target primarily inhibitory $pTRN^{ADRB1}$ neurons, we injected AAV9.hSyn.Con/Fon.hChR2(H134R).EYFP into the pTRN of ADRB1-Cre;Vgat-Flp mice to restrict ChR2 expression to $pTRN^{ADRB1;VGAT}$ neurons. Stimulation of $pTRN^{ADRB1;VGAT}$ neurons only slightly increased wakefulness (Fig. 4 *D*–*F*). As controls, we stimulated all CaMKIIa-expressing pTRN neurons and found that the stimulation was sufficient to promote wakefulness but not to the level of $pTRN^{ADRB1;CaMKIIa}$ activation (Fig. 4 *G*–*I*). In addition, stimulation of $VGAT^{+}$ non-$ADRB1^{+}$ pTRN neurons did not affect sleep–wake state (Fig. 4 *J*–*L*). These results together suggest that excitatory $pTRN^{ADRB1}$ neurons are primarily responsible for the wake-promoting phenotype of $pTRN^{ADRB1}$ neurons.

Characterizing pTRN Neurons by Projection Pattern. After establishing that $pTRN^{ADRB1}$ neurons can affect sleep–wake state, we next examined how pTRN neurons integrate into the larger sleep circuitry. We hypothesized that groups of pTRN neurons exist that can be distinguished by their projection patterns to known sleep–wake circuitries. To test this hypothesis, we used MAPseq which determines the neuron projection motifs by sequencing RNA barcodes. Briefly, a Sindbis virus with 2 million unique barcodes was first injected into the pTRN. Subsequently, the pTRN and eight sleep–wake regions that received pTRN input were dissected out and sequenced in order to find projection motifs (Fig. 5*A*). With the barcodes, we can directly correlate the output targets to individual projection neurons. We found that more than 40% of the projection neurons projected to just one of the eight regions and that

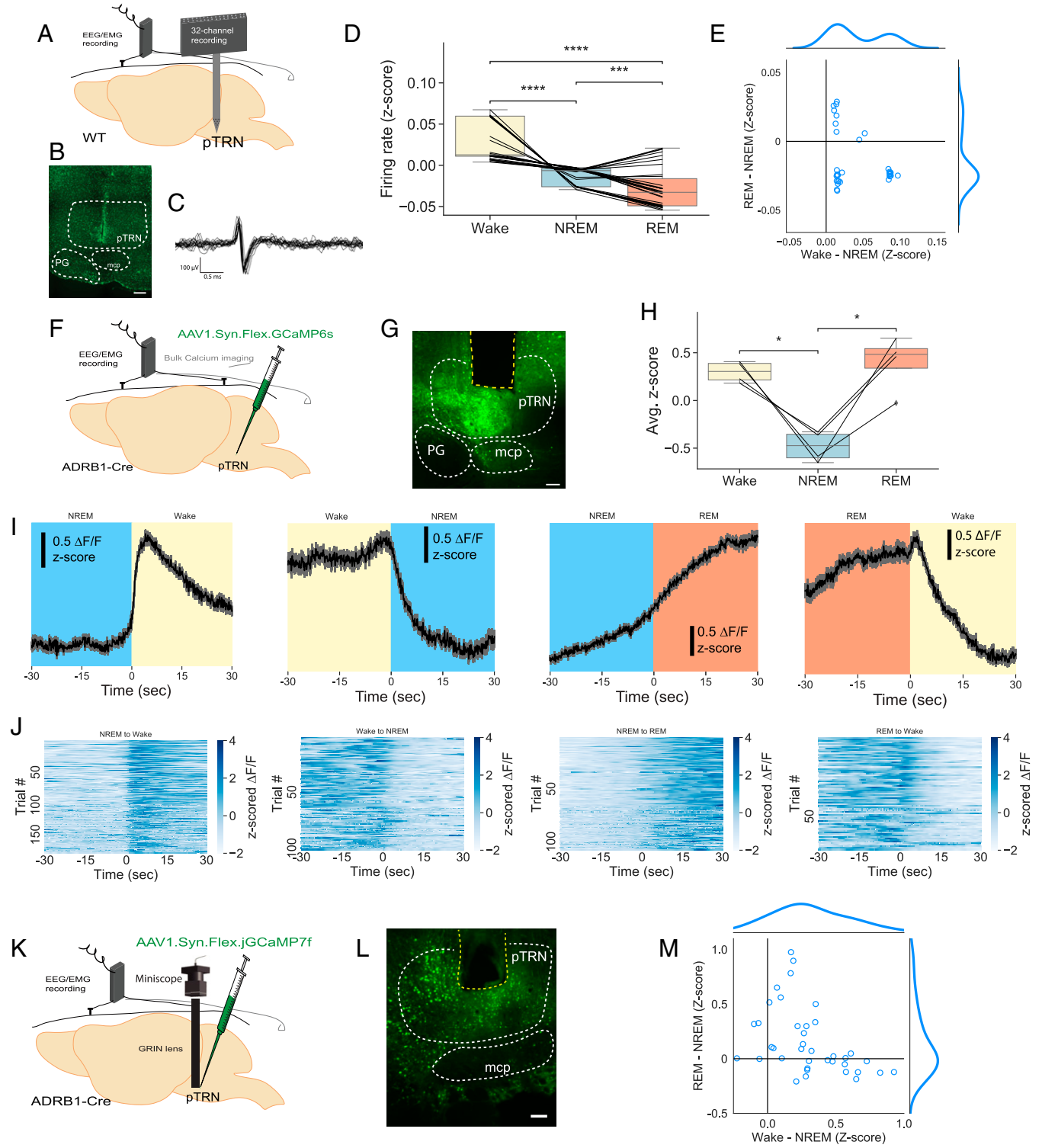

Fig. 2. Endogenous activity of pTRN neurons. (*A*) Experimental schematic for simultaneous 32-channel electrophysiology and EEG/EMG recording. (*B*) Histology showing silicon probe placement stained with Cd11b (green), a marker for microglia, which are activated near the probe track. (Scale bar, 200 µm.) (*C*) Trace of 20 spikes from a representative unit. (*D*) The Z-scored firing rate of the isolated units between sleep states from WT mice (n = 3 mice, n = 34 units) (wake vs. NREM: $P < 0.0001$, wake vs. REM: $P < 0.0001$, NREM vs. REM: $P = 0.0002$, repeated measures one-way ANOVA with post hoc Sidak's multiple comparisons test, ***$P < 0.001$, ****$P < 0.0001$). See also *SI Appendix*, Fig. S4. (*E*) REM–NREM activity difference vs. wake–NREM activity difference from *D*. Each circle represents one unit. (*F*) Experimental schematic for imaging bulk calcium fluorescence from pTRN^{ADRB1} neurons. (Scale bar, 50 µm.) (*G*) Histology showing the probe track (outlined in yellow) combined with GCaMP signal. (Scale bar, 150 µm.) (*H*) Z-scored fluorescence vs. sleep–wake state from ADRB1-Cre mice (n = 4) injected with AAV1.Syn.Flex.GCaMP6s (wake vs. NREM: $P = 0.0310$, wake vs. REM: $P = 0.6024$, NREM vs. REM: $P = 0.0310$, repeated measures one-way ANOVA with post hoc Sidak's multiple comparisons test, *$P < 0.05$). (*I*) Z-scored calcium fluorescence peristimulus time histograms for NREM-to-wake (n = 191), wake-to-NREM (n = 107), NREM-to-REM (n = 114), and REM-to-wake (n = 73) transitions averaged over all trials across n = 4 mice. Gray bars represent SEM. (*J*) Z-scored heatmaps from *I*. The intensity of blue corresponds with the ΔF/F value. (*K*) Experimental setup for imaging pTRN^{ADRB1} neurons using a miniscope. (*L*) The probe track (outlined in yellow) above pTRN^{ADRB1} neurons expressing GCaMP7f. (Scale bar, 200 µm.) (*M*) REM–NREM activity difference vs. wake–NREM activity difference. Each circle represents one cell (n = 4 mice, n = 38 cells). For *D* and *H*, the boxes show the quartiles, and the whiskers show the rest of the distribution. PG, pontine gray; mcp, middle cerebellar peduncle.

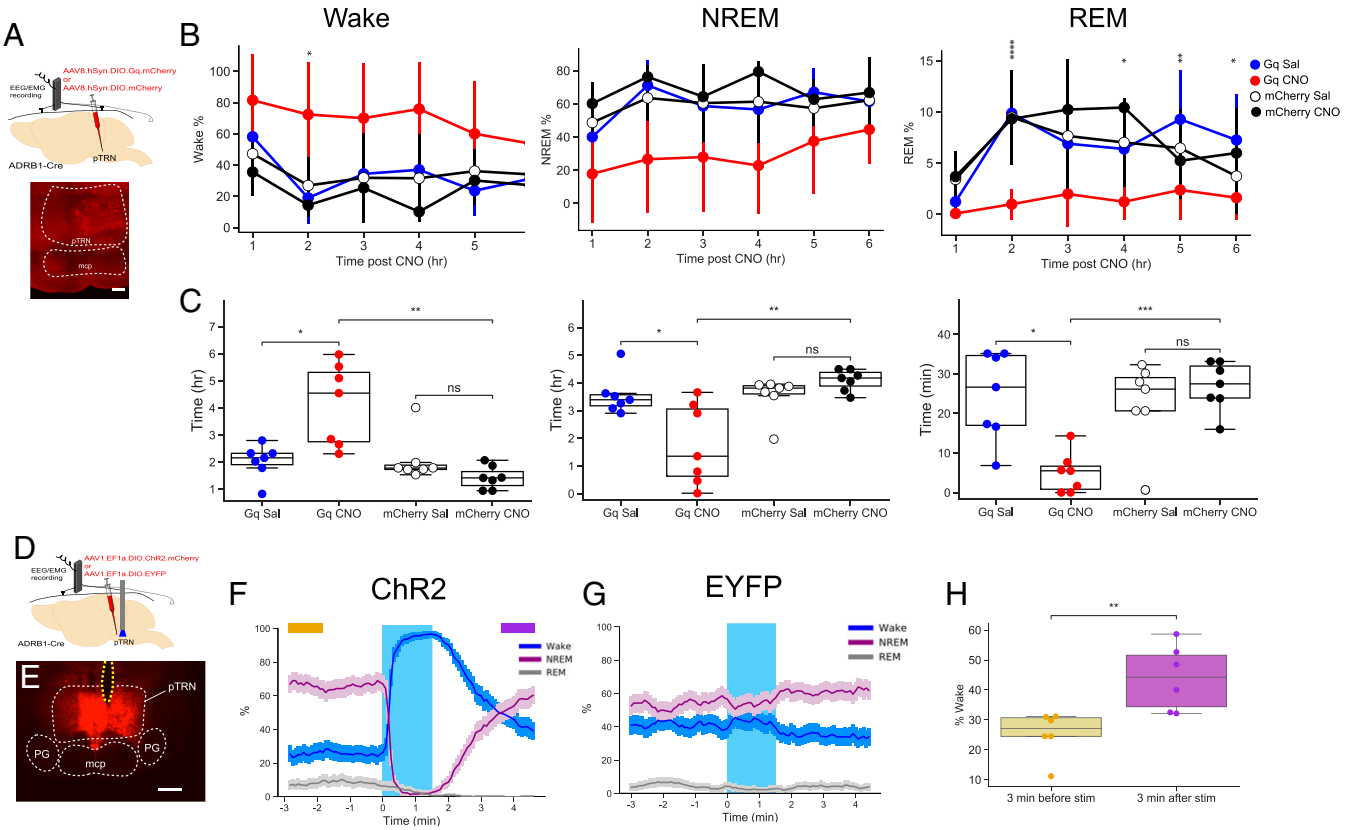

Fig. 3. Activation of pTRN^{ADRB1} neurons promotes wakefulness. (*A, Top*) Schematic to express Gq or mCherry in pTRN^{ADRB1} neurons. (*Bottom*) Representative histology. (Scale bar, 400 μm.) (*B*) Hour-by-hour quantification of time spent in wake (*Left*), NREM (*Middle*), or REM (*Right*) in Gq (n = 7) or mCherry (n = 7) mice for 6 h post-CNO or saline injection at ZT1 (Gq-Sal vs. Gq-CNO, two-way RM ANOVA with post hoc Sidak's multiple comparisons test, *P < 0.05, **P < 0.01, ****P < 0.0001). (*C*) Total time in the 6-h postinjection period spent in wake (*Left*), NREM (*Middle*), and REM (*Right*) from *B* (wake Gq-Sal vs. Gq-CNO: P = 0.0240, wake Gq-CNO vs. mCherry-CNO: P = 0.0053, wake mCherry-Sal vs. mCherry-CNO: P = 0.1219; NREM Gq-Sal vs. Gq-CNO: P = 0.0432, NREM Gq-CNO vs. mCherry-CNO: P = 0.0109, NREM mCherry-Sal vs. mCherry-CNO: P = 0.2933; REM Gq-Sal vs. Gq-CNO: P = 0.0247, REM Gq-CNO vs. mCherry-CNO: P = 0.0002, REM mCherry-Sal vs. mCherry-CNO: P = 0.7925, repeated measures one-way ANOVA with post hoc Sidak's multiple comparisons test, ns P > 0.05, *P < 0.05, **P < 0.01, ***P < 0.001). See also *SI Appendix*, Figs. S5 and S6. (*D*) Schematic showing the setup to express ChR2 or EYFP in pTRN^{ADRB1} neurons. (*E*) Histology showing probe track (outlined in yellow) in the pTRN. (Scale bar, 400 μm.) (*F*) Effect of optogenetic activation (n = 6 mice, n = 300 trials). The blue stripe shows when the light-emitting diode (LED) is on (20 Hz, 90 s). Error bars represent the 95% confidence interval from 10,000 iterations. LED stimulation increased wake and decreased NREM and REM. Yellow and purple bars are for time periods analyzed in *H* (increase in wake: P < 0.0001, decrease in NREM: P < 0.0001, decrease in REM: P = 0.0001, bootstrap). See also *SI Appendix*, Fig. S7. (*G*) Same as in *F* but for EYFP-injected mice (n = 6 mice, n = 300 trials). There was no change in sleep–wake states when analyzed by bootstrapping (increase in wake: P = 0.0768, decrease in NREM: P = 0.2358, decrease in REM: P = 0.1225, bootstrap). (*H*) LED stimulation was able to increase the percentage of wakefulness 2 to 3 min after stimulation (purple) compared with 2 to 3 min before stimulation (yellow) from *F*. The time periods from *F* analyzed are denoted with yellow and purple bars (3 min before vs. 3 min after, P = 0.0063, Student's two-sided t test, **P < 0.01). Error bars represent ± SEM for *B*. For *C* and *H*, the boxes show the quartiles, and the whiskers show the rest of the distribution. mcp, middle cerebellar peduncle; PG, pontine gray.

>90% of the neurons projected to four or fewer regions (Fig. 5*B*). Using principal component analysis (PCA) on the projection neurons, we identified at least three groups of projection neurons (Fig. 5*C*). Further investigation of the MAPseq data suggested that pTRN projection neurons could be divided into anterior-projecting and posterior-projecting neurons (Fig. 5 *D* and *E*). Of the neurons that projected anteriorly to the lateral hypothalamus (LH), 22% also projected posteriorly to the parafacial zone (PZ) (Fig. 5*D*). Conversely, of neurons that projected to the PZ, 15% also projected to the LH (Fig. 5*E*). Thus, we concluded that LH-projecting and PZ-projecting neurons are roughly distinct groups. Retrobead tracing with CTb (cholera toxin b) injections in the LH and PZ showed little overlap in the pTRN, further suggesting that LH-projecting and PZ-projecting neurons have little overlap (*SI Appendix*, Fig. S10). Motifs with the highest count number tended to either include the ventrolateral periaqueductal gray (vlPAG) or the ventral tegmental area (VTA), regions that are anatomically closest to the pTRN (Fig. 5 *F* and *G*). Consistent with these findings, injection of a Cre-dependent synaptophysin virus, which primarily labels sites of presynaptic vesicle release, into the pTRN of ADRB1-Cre mice revealed that the projections of pTRN^{ADRB1} neurons were concentrated in the hypothalamus, brainstem, and midbrain (Fig. 5 *H–J*). Collectively, these data revealed that the pTRN contains a mixture of different neurons projecting to various sleep-relevant brain areas and that these neurons can be roughly divided into anterior-projecting and posterior-projecting neurons. In addition, pTRN^{ADRB1} neurons mainly project to the hypothalamus, brainstem, and midbrain.

Output Circuits of pTRN^{ADRB1} Neurons. We next investigated the functional connections of pTRN^{ADRB1} neurons with downstream regions. Based on our finding that pTRN^{ADRB1} neurons project to the LH (Fig. 5*J*), we hypothesized that pTRN^{ADRB1}→LH projections play a role in the wake-promoting effect of pTRN^{ADRB1} neurons. We first investigated the endogenous activity of pTRN^{ADRB1} projections to the LH. We injected a next generation calcium sensor, AAV1.Syn.Flex.GCaMP7s, which is bright enough to be viewed at the axon terminal, into the pTRN of ADRB1-Cre mice and placed a fiber optic cannula above the LH (Fig. 6 *A* and *B*). We found that pTRN^{ADRB1}→LH projections had the highest ΔF/F activity

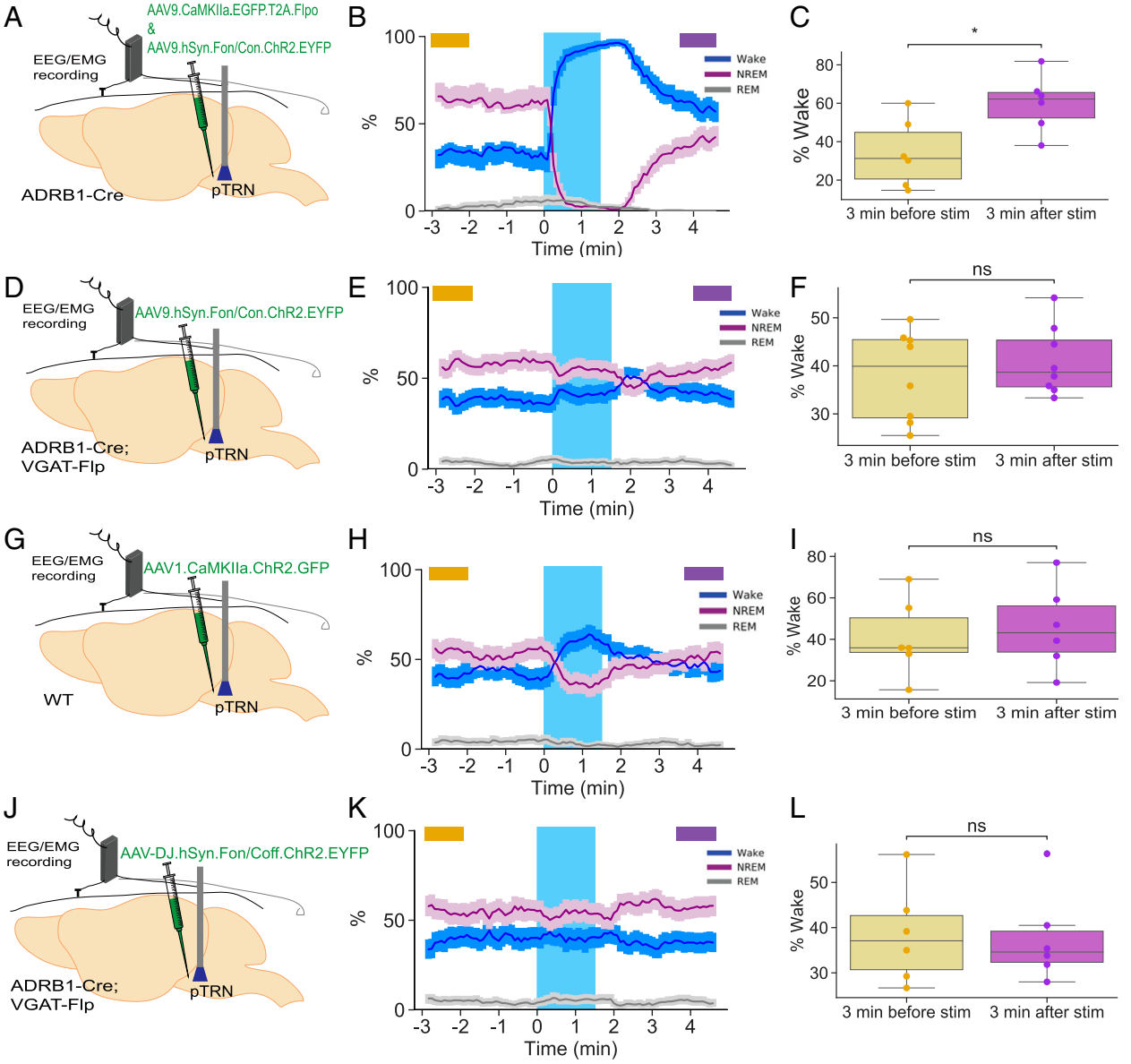

Fig. 4. Excitatory pTRN^{ADRB1} neurons promote wake. (*A*) Schematic showing the approach to express ChR2 in excitatory pTRN^{ADRB1} neurons. (*B*) Effect of optogenetic activation (n = 6 mice, n = 275 trials). The blue stripe shows when the LED is on (20 Hz, 90 s). Error bars represent the 95% confidence interval from 10,000 iterations. LED stimulation increased wake, decreased NREM, and led to no change in REM. Yellow and purple bars are for time periods analyzed in *C* (increase in wake: $P < 0.0001$, decrease in NREM: $P < 0.0001$, decrease in REM: $P = 0.40$, bootstrap). See also *SI Appendix*, Fig. S9. (*C*) LED stimulation was able to increase the percentage of wakefulness 2 to 3 min after stimulation (purple) compared with 2 to 3 min before stimulation (yellow) from *B*. The time periods analyzed from *B* are denoted with yellow and purple bars (3 min before vs. 3 min after, $P = 0.0203$, Student's two-sided t test, $^*P < 0.05$). (*D*) Schematic showing the approach to activating inhibitory pTRN^{ADRB1} neurons. (*E*) LED stimulation led to a slight increase in wake, a decrease in NREM, and no change in REM. Yellow and purple bars are for time periods analyzed in *F* (n = 6 mice, n = 300 trials) (wake: $P = 0.0046$, NREM: $P = 0.0039$, REM: $P = 0.683$, bootstrap). (*F*) Quantification of yellow and purple bar time periods from *E* (3 min before vs. 3 min after, $P = 0.48$, Student's two-sided t test, ns $P > 0.05$). (*G*) Approach to stimulating all excitatory pTRN neurons as a control for *A*. (*H*) Effect of LED stimulation (n = 6 mice, n = 300 trials) for *G*. LED stimulation led to an increase in wake and decreases in NREM and REM (increase in wake: $P < 0.0001$, decrease in NREM: $P < 0.0001$, decrease in REM: $P = 0.0217$, bootstrap). Yellow and purple bars are for time periods analyzed in *I*. (*I*) Quantification of yellow and purple bar time periods from *H* (3 min before vs. 3 min after, $P = 0.68$, Student's two-sided t test, ns $P > 0.05$). (*J*) Schematic showing the approach to expressing ChR2 in inhibitory non-ADRB1 pTRN neurons as a control for *D*. (*K*) Effect of LED stimulation (n = 6 mice, n = 295 trials) for *J*. LED stimulation led to no change in wake, NREM, or REM state (increase in wake: $P = 0.4423$, decrease in NREM: $P = 0.2784$, decrease in REM, $P = 0.9159$, bootstrap). Yellow and purple bars are for time periods analyzed in *L*. (*L*) Quantification of yellow and purple bar time periods from *K* (3 min before vs. 3 min after, $P = 0.91$, Student's two-sided t test, ns $P > 0.05$). Error bars represent the 95% confidence interval from 10,000 iterations for *B*, *E*, *H*, and *K*. For *C*, *F*, *I*, and *L* the boxes show the quartiles, and the whiskers show the rest of the distribution.

during wake and REM (Fig. 6*C*). Investigation of sleep–wake transitions revealed that ΔF/F activity increased during NREM-to-wake and NREM-to-REM transitions and decreased during wake-to-NREM transitions (Fig. 6 *D* and *E*). Activity was biphasic for REM-to-wake transitions, first increasing and then decreasing (Fig. 6 *D* and *E*). These results are reminiscent of our observations of endogenous activity of pTRN^{ADRB1} neurons at the cell body (Fig. 2 *I* and *J*). Next, to test whether activation of pTRN^{ADRB1}→LH terminals was sufficient to promote wakefulness, we injected AAV1.EF1a.DIO.ChR2 into the pTRN of ADRB1-Cre mice and implanted a fiber optic probe above the LH (Fig. 6 *F* and *G*). Stimulation at 20 or 10 Hz was sufficient to promote wakefulness from either NREM or REM sleep (Fig. 6*H* and *SI Appendix*, Figs. S11 and S12).

Several LH neuron subtypes have been shown to participate in sleep–wake regulation. Histological analysis suggested that

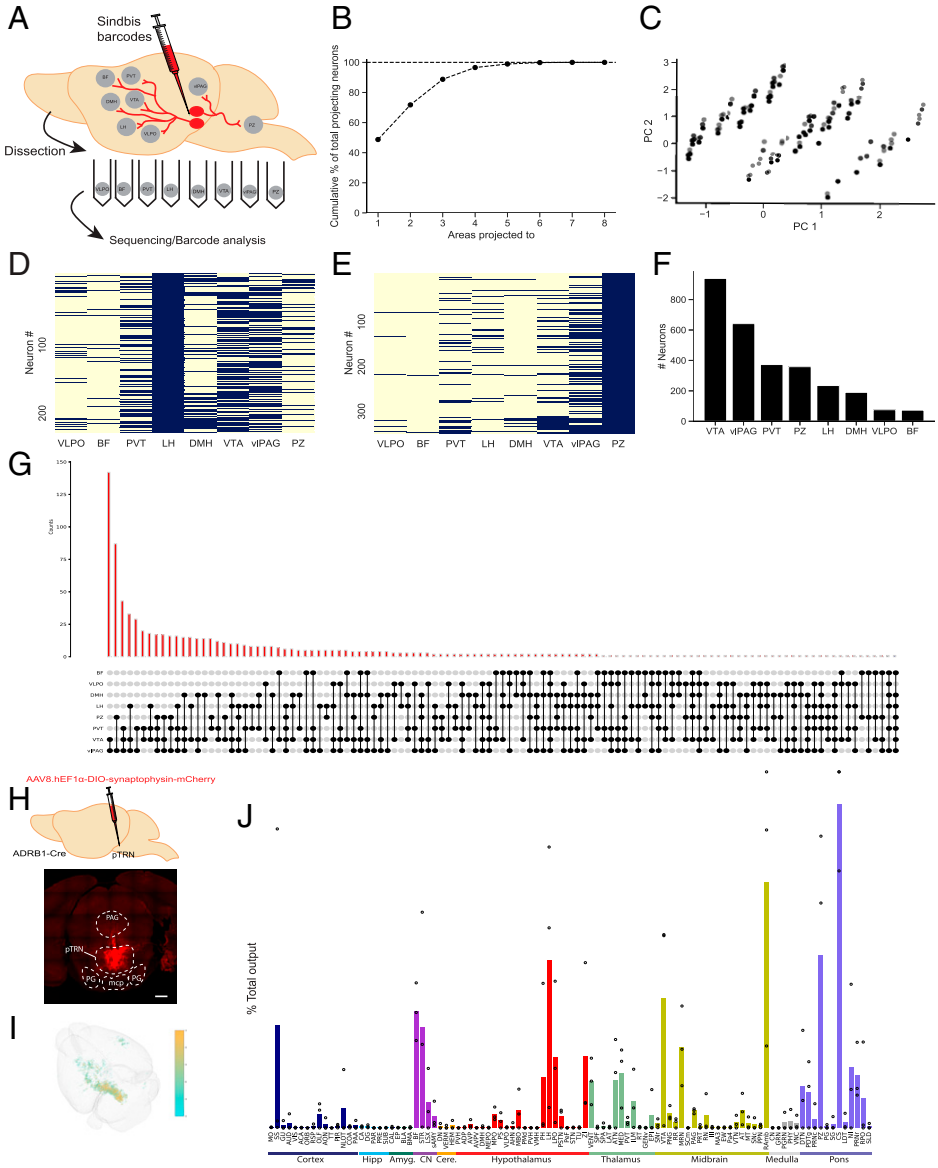

Fig. 5. Projection patterns of pTRN neurons. (*A*) MAPseq overview. Briefly, a barcoded Sindbis virus was injected, and eight brain regions (gray circles) involved in sleep–wake regulation were dissected 42 h later for sequencing and subsequent analysis. (*B*) The cumulative percentages of neurons that project to the sleep–wake brain areas were analyzed. Nearly all neurons projected to four or fewer areas. (*C*) PCA of the projection neurons from a binarized projection matrix. (*D*) Heatmap of different areas to which the LH-projecting neurons also projected. (*E*) Heatmap of different areas to which the PZ-projecting neurons also projected. See also *SI Appendix*, Fig. S10. (*F*) The number of pTRN neurons projecting to each projection region. (*G*) Count number for pTRN projection motifs. (*H*, *Top*) Schematic of the approach for tracing $pTRN^{ADRB1}$ processes through the entire brain. (*Bottom*) Representative image of the pTRN injection site. (Scale bar, 400 μm.) (*I*) Example of a three-dimensional reconstruction of $pTRN^{ADRB1}$ input to the brain by signal intensity. (*J*) Quantification of the relative input from $pTRN^{ADRB1}$ neurons to different brain regions (n = 3 mice). Nomenclature adopted from the Allen Brain Atlas: ACA, anterior cingulate area; ADP, anterodorsal preoptic nucleus; AHN, anterior hypothalamic nucleus; AON, anterior olfactory nucleus; AT, anterior tegmental nucleus; ATN, anterior group of the dorsal thalamus; AUD, auditory areas; AVP, anteroventral preoptic nucleus; AVPV, anteroventral periventricular nucleus; BF, basal forebrain; BLA, basolateral amygdala; BMA, basomedial amygdala; CA, Ammon's horn; CAL, claustrum; CN, cochlear nuclei; COA, cortical amygdala area; CS, superior central nucleus raphe; DG, dentate gyrus; DMH, dorsomedial hypothalamus; DN, dentate nucleus; DTN, dorsal tegmental nucleus; EP, endopiriform nucleus; EPI, epithalamus; EW, Edinger-Westphal nucleus; GENv, geniculate group, ventral thalamus; GRN, gigantocellular reticular nucleus; GU, gustatory areas; HEM, hemispheric regions; III, ocularmotor nucleus; ILM, intralaminar nuclei of the dorsal thalamus; LAT, lateral group of the dorsal thalamus; LDT, laterodosal tegmental nucleus; LH, lateral hypothalamus; LPO, lateral preoptic nucleus; LSX, lateral septal complex; MA3, medial accessory oculomotor nucleus; MBO, mammillary body; MED, medial group of the dorsal thalamus; MEPO, median preoptic nucleus; mcp, middle cerebellar peduncle; MO, somatomotor areas; MPO, medial preoptic nucleus; MRN, midbrain reticular nucleus; MT, medial terminal nucleus of the accessory optic tract; NI, nucleus incertus; NLOT, nucleus of the lateral olfactory tract; OLF, olfactory areas; ORB, orbital area; Pa4, paratrochlear nucleus; PAA, piriform amygdalar area; PAG, periaqueductal gray; PAR, parasubiculum; PDTg, posterodorsal tegmental nucleus; PeF, perifornical nucleus; PG, pontine gray; PGRN, paragigantocellular reticular nucleus; PH, posterior hypothalamic nucleus; PHY, perihypoglossal nuclei; PIR, piriform area; PMd, dorsal premammillary nucleus; PNG, paranigral nucleus; PPN, pedunculopontine nucleus; PRE, presubiculum; PRNc, pontine reticular nucleus-ventral part; PRNr, pontine reticular nucleus; PRT, pretectal region; PS, parastrial nucleus; PSTN, parasubthalamic nucleus; PVH, paraventricular hypothalamic nucleus; PVT, paraventricular nucleus of the thalamus; PZ, parafacial zone; RAmb, midbrain raphe nuclei; RN, red nucleus; RPO, nucleus raphe pontis; RR, midbrain reticular nucleus-retrorubral area; RSP, retrosplenial area; RT, reticular nucleus of the thalamus; sAMY, striatum-like amygdalar nuclei; SCm, superior colliculus, motor related; SG, supragenual nucleus; SLD, sublaterodorsal nucleus; SNc, substantia nigra—compact part; SNr, substantia nigra—reticular part; SPA, subparafascicular area; SPF, subparafascicular nucleus; SS, somatosensory areas; STN, subthalamic nucleus; STR, striatum; SUB, subiculum; TT, taenia tecta; TU, tuberal nucleus; VENT, ventral group of the dorsal thalamus; VERM, vermal regions; VIS, visual areas; VLPO, ventrolateral preoptic nucleus; VMH, ventromedial hypothalamic nucleus; VNC, vestibular nuclei; VTA, ventral tegmental area; VTN, ventral tegmental nucleus; ZI, zona incerta.

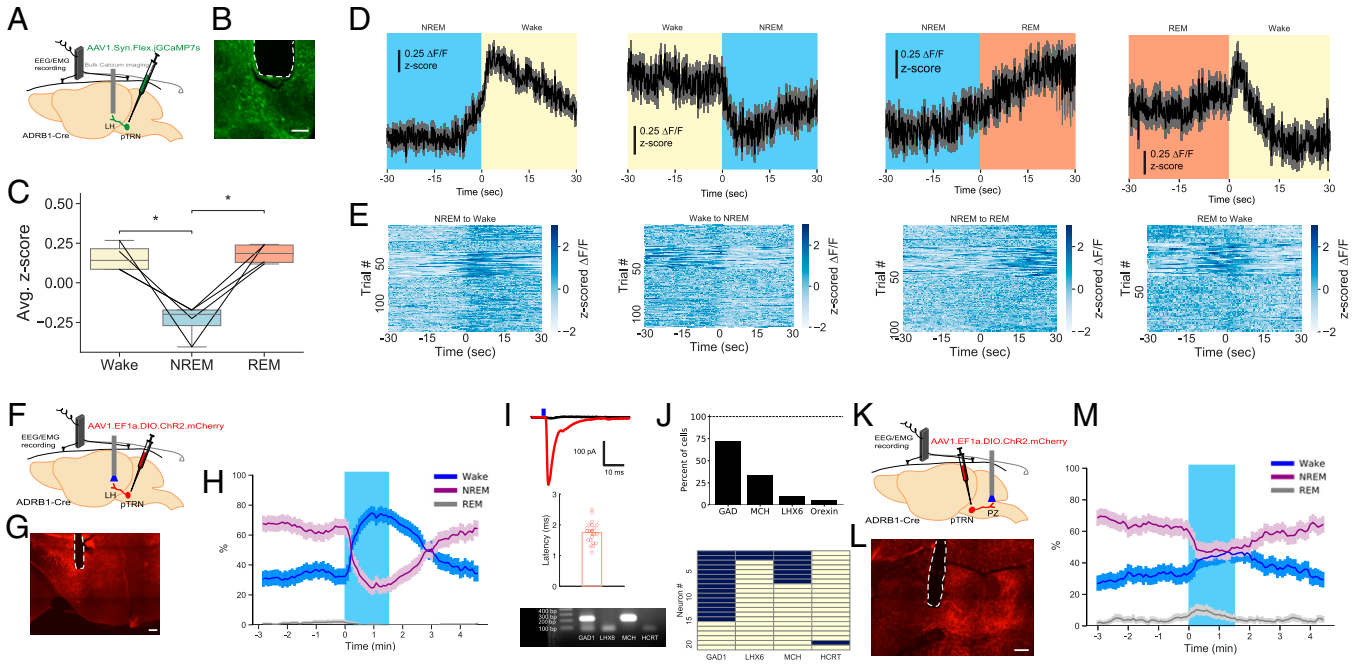

Fig. 6. Output circuits of pTRN^{ADRB1} neurons. (*A*) Schematic for imaging pTRN^{ADRB1}→LH axons. (*B*) Histology showing the probe track (outlined in white) above the pTRN^{ADRB1} processes (green). (Scale bar, 200 μm.) (*C*) Z-scored ΔF/F of pTRN^{ADRB1}→LH terminals. The box shows the quartiles, and the whiskers show the rest of the distribution (wake vs. NREM: $P = 0.023$, wake vs. REM: $P = 0.0264$, repeated measures one-way ANOVA with post hoc Sidak's multiple comparisons test, $^*P < 0.05$). (*D*) Z-scored calcium fluorescence peristimulus time histograms for NREM-to-wake, wake-to-NREM, NREM-to-REM, and REM-to-wake transitions, averaged over all trials. Gray bars represent SEM. (*E*) Z-scored heatmaps from *D*. The intensity of blue corresponds to the ΔF/F value. (*F*) Schematic showing the strategy to activate pTRN^{ADRB1} axons in the LH. (*G*) Histology showing the probe track (outlined in white) near the pTRN^{ADRB1} axons (red). (Scale bar, 200 μm.) (*H*) Effect of optogenetic activation ($n = 6$ mice, $n = 300$ trials). The blue stripe shows when the LED is on (20 Hz, 90 s). Error bars represent the 95% confidence interval from 10,000 iterations. LED stimulation increased wake and decreased NREM and REM (increase in wake: $P < 0.0001$, decrease in NREM: $P < 0.0001$, decrease in REM: $P = 0.0003$, bootstrap). See also *SI Appendix*, Figs. S11 and S12. (*I*, *Top*) pTRN^{ADRB1} neurons were injected with ChR2, and an acute slice was taken from the LH. In the example trace of a patched neuron from an acute LH slice, blue denotes when the blue LED was on, and the inward current from the patched neuron is shown in red. The black trace is the same neuron but with the excitatory blockers CNQX (20 μM) and APV (50 μM). (*Middle*) The latency between LED stimulation and inward current deflection for the 21 connected neurons. (*Bottom*) Example gel for the single-cell RT-PCR for the four genes examined. (*J*, *Top*) Percentages of each of the connected cells expressing each gene ($n = 3$ mice, $n = 21$ cells). (*Bottom*) A matrix showing the expression and overlap of each gene for each individual connected cell. See also *SI Appendix*, Fig. S13. (*K*) Schematic showing the strategy to activate pTRN^{ADRB1} terminals in the PZ. (*L*) Example of a histology image of the probe track (outlined in white) and fibers (red) in the PZ. (Scale bar, 200 μm.) (*M*) Effect of optogenetic activation ($n = 6$ mice, $n = 300$ trials). LED stimulation increased wake and REM and decreased NREM (increase in wake: $P < 0.0001$, decrease in NREM: $P < 0.0001$, increase in REM: $P = 0.0002$, bootstrap).

pTRN^{ADRB1} neuron fibers were near HCRT-expressing and melanin-concentrating hormone (MCH)-expressing cells, but fiber proximity does not necessarily imply synaptic connectivity (*SI Appendix*, Fig. S13). To directly determine which of the LH subtypes are connected to pTRN^{ADRB1} neurons, we next utilized channelrhodopsin-assisted circuit mapping (CRACM). We again expressed ChR2 in pTRN^{ADRB1} neurons and cut an acute slice of the LH. After whole-cell patch clamp of LH neurons, blue light stimulation was applied to the brain slice. Individual cells were isolated if we were able to establish a short latency from light application to inward current. The individual cells were then further analyzed by RT-PCR (Fig. 6*I*). We found that the majority (15/21) of connected neurons were GAD1-positive, though MCH-positive neurons (7/21) were also connected (Fig. 6*J*). A small number of neurons were LHX6-positive (2/21) and HCRT-positive (1/21) (Fig. 6*J*). Together, these results indicate that pTRN^{ADRB1}→LH stimulation increases wakefulness and that pTRN^{ADRB1} neurons primarily promote wakefulness through LH^{GAD1} neurons.

Finally, based on the anatomical segregation seen in projection patterns, we investigated the effect of stimulating pTRN^{ADRB1}→PZ neurons (Fig. 6 *K* and *L*). Similar to pTRN^{ADRB1}→LH stimulation, pTRN^{ADRB1}→PZ stimulation led to an increase in wakefulness, but pTRN^{ADRB1}→PZ stimulation also led to an increase in REM (Fig. 6*M*). Overall, these studies demonstrate the functional divergence of pTRN^{ADRB1}→LH and pTRN^{ADRB1}→PZ projections while establishing the role of pTRN^{ADRB1} neurons in the larger framework of sleep–wake circuitry.

Discussion

We began our study by recognizing that ADRB1-positive neurons in one area or multiple areas of the brain must influence the sleep–wake state. Although we reported a sleep–wake modulating role for ADRB1-positive neurons in the DP, a critical question requiring further investigation was whether additional regions are important. We thus set out to identify additional ADRB1-positive neurons/regions involved in sleep duration regulation. This study establishes a role for the pTRN in sleep regulation, setting the groundwork for future research. The role of the pTRN in behavior has also not been well established. This study should provide a baseline for future elucidation of the role (if any) of the pTRN in other behaviors.

Ablating pTRN^{ADRB1} neurons led to a ∼3-h increase in total wake duration over a 24-h period. This is a moderate effect size compared with ventrolateral preoptic nucleus (VLPO) (4) and PZ (3) ablation (∼6-h increase in wake time in rats), LH^{MCH} (10, 23), and pIII^{CALCA} (13) neuron ablation (∼1.5-h increase in wake time in mice), RMTg neuron ablation (24) (∼1.5-h

increase in wake time in rats), and VTA^{GABA} neuron ablation (12) (~4-h increase in total wake time in mice). The results presented here suggest that the pTRN is a crucial brain area regulating wake duration.

This 3-h increase in wake time was caused by an increase in wake-to-wake epoch transition probability with a corresponding decrease in wake-to-NREM epoch transition probability, suggesting that $pTRN^{ADRB1}$ neurons may be involved in wake maintenance. Evidence that $pTRN^{ADRB1}$ neurons are involved in wake maintenance is further supported by our activation experiments. Acute optogenetic activation for 90 s was sufficient to lead to an increase in wake probability 2 to 3 min after stimulation offset when compared with the prestimulation period. Furthermore, at ZT1, when the mice are awake nearly 80% of the time with a saline injection, Gq activation of $pTRN^{ADRB1}$ neurons was able to further increase their wake percentage. Thus, stimulation of $pTRN^{ADRB1}$ neurons on both the second and minute timescales can alter the state of the brain after activation ends, suggesting that $pTRN^{ADRB1}$ neurons can affect the network regulating sleep and wakefulness.

Studying nuclei in poorly characterized brain regions is difficult (in part) due to the lack of genetic mouse lines in which each nucleus is distinctly labeled. Our ADRB1-Cre line is not specific to the pTRN, and thus, there is the possibility of some viral expression in ADRB1-positive neurons outside of the pTRN. To control for this possibility, we have employed a wide range of techniques with varying degrees of specificity. Although DREADDs lack spatial precision, we subsequently relied on optogenetics, which has more temporal and spatial precision. In addition, photometry and single-cell imaging experiments are more spatially localized. Finally, to control for viral spread, we injected just 50 nL of TeNT virus and found a similar result to our caspase ablation experiments. Together, these results strongly indicate that our target is primarily the pTRN. In subsequent studies, single-cell sequencing can be used to find a genetic marker that only labels the pTRN in order to parse the function of these neurons in greater detail.

The natural activity of $pTRN^{ADRB1}$ neurons was high during wake and REM sleep at both the population and single-cell levels, suggesting $pTRN^{ADRB1}$ neurons are wake- and REM-active. Furthermore, activation using DREADDs or optogenetics led to increases in wakefulness, suggesting $pTRN^{ADRB1}$ neurons are wake-promoting. However, ablation of $pTRN^{ADRB1}$ neurons led to an increase in wakefulness, contrasting with the notion that $pTRN^{ADRB1}$ neurons are wake-promoting. Initially, we hypothesized that we might be targeting a mixture of neurons, but our combinatorial genetics strategy and targeting different populations of pTRN neurons by projection patterns did not reveal a population of NREM-promoting or NREM-active cells. Moreover, injecting 50 nL of TeNT virus labeled a small number of neurons yet still led to an increase in total wake duration. We therefore conclude that $pTRN^{ADRB1}$ neurons are wake- and REM-active, but that chronic silencing or ablating $pTRN^{ADRB1}$ neurons leads to increases in wakefulness. Thus, $pTRN^{ADRB1}$ neurons escape straightforward characterizations as either wake-promoting or sleep-promoting. Similar to our results, VGLUT2-positive neurons in the basal forebrain show high activity during wakefulness and REM sleep and promote wakefulness when acutely stimulated yet lead to an increase in wakefulness when ablated (25, 26). We suggest that interpreting the function of neurons as wake-promoting or sleep-promoting may depend on the experimental technique and timescale of the manipulation. How then do we propose that the $pTRN^{ADRB1}$ neurons promote wake when acutely stimulated yet lead to increases in total wake time when chronically ablated? It is well established that neural damage or lesions can cause difficult-to-predict dysregulation of other brain areas. We hypothesize that while acute activity suggests $pTRN^{ADRB1}$ neurons are wake-promoting, chronically removing $pTRN^{ADRB1}$ neurons may cause permanent changes in downstream circuitry. We showed that $pTRN^{ADRB1}$ neurons send relatively strong projections to many brainstem and hypothalamic areas involved in sleep–wake regulation, and thus, it is possible that chronically removing $pTRN^{ADRB1}$ neuron input causes dysregulation of downstream sleep–wake circuitry. Therefore, it is crucial to study the effect of $pTRN^{ADRB1}$ neuron ablation on the activity of downstream sleep–wake circuitries in future studies.

We used combinatorial genetics to investigate the contributions of the $pTRN^{ADRB1;CaMKIIa}$ neurons and $pTRN^{ADRB1/VGAT}$ neurons on sleep–wake behavior. Unexpectedly, the commercially available VGLUT2-Flp mouse had weak Flp-mediated expression in the pTRN, possibly due to the design of the mouse line using internal ribosome entry site (IRES), which can lead to lower expression compared with other approaches such as T2A. To circumvent this issue, we acquired a custom-made virus that expresses Flp under the CaMKIIa promoter. We found that activating $pTRN^{ADRB1;CaMKIIa}$ neurons promoted wakefulness and that stimulating $pTRN^{ADRB1/VGAT}$ neurons produced a weaker effect. In the future, it would be useful to generate a VGLUT2-Flp mouse with stronger Flp expression. Overall, these combinatorial genetic experiments uncovered different effects for neuronal subtypes.

Another approach to dissect neuronal heterogeneity is through characterization of different projection patterns. We employed MAPseq, a recently developed technology that uses RNA barcodes, to directly investigate the projection motifs of pTRN neurons. Although the MAPseq experiment revealed pTRN but not $pTRN^{ADRB1}$ projections, due to the lack of Cre-driven specificity, our preliminary and subsequent synaptophysin tracing for $pTRN^{ADRB1}$ neurons showed projections to the MAPseq projection regions selected for sequencing. With MAPseq, we identified at least two groups of neurons, those that project anteriorly and those that project posteriorly, a finding supported by retrobead tracing. Crucially, we found that this projection pattern subdivision also had functional consequences. While both the PZ- and LH-projecting $pTRN^{ADRB1}$ neurons promoted wakefulness, the PZ-projecting $pTRN^{ADRB1}$ neurons weakly promoted REM sleep. Thus, MAPseq is suitable for identifying functionally distinct neuronal populations.

We showed that $pTRN^{ADRB1}$ neurons project to many known sleep areas and that $pTRN^{ADRB1}$ neurons promote wake (in part) through their projection to the LH. Furthermore, $pTRN^{ADRB1}$ projections to the LH showed the highest calcium activity during wake and REM. Interestingly, the $\Delta F/F$ increase between NREM and wake in the projections preceded the NREM-to-wake transition, perhaps suggesting that $pTRN^{ADRB1} \rightarrow LH$ projections may endogenously drive NREM-to-wake transitions. Using CRACM, we found that $pTRN^{ADRB1}$ neurons were monosynaptically connected primarily to LH^{GAD1} neurons (~70% of connected cells). Consistent with our results, LH^{GAD1} neurons have previously been shown to promote wakefulness when stimulated (27, 28). These results establish the $pTRN^{ADRB1} \rightarrow LH^{GAD1}$ as part of the wake-promoting circuitry and places the pTRN squarely in the sleep–wake network. Notably, stimulating $pTRN^{ADRB1}$ terminals in the LH promoted wakefulness, but not to the nearly 100% seen for cell body stimulation, indicating that $pTRN^{ADRB1}$ neurons promote wakefulness through other brain

areas besides the LH (e.g., PZ). In addition, we found weaker but statistically significant effects of wake promotion from stimulating pTRN^{ADRB1}→PZ projections. These results suggest that stimulation of pTRN^{ADRB1}→LH projections may be more important than stimulation of pTRN^{ADRB1}→PZ projections for promoting wake.

In summary, the results of this study showed that pTRN^{ADRB1} neurons are wake-active and potent promoters of wakefulness. Moreover, activation of these neurons promotes wakefulness well after the end of stimulation. We used combinatorial genetics to show that excitatory pTRN^{ADRB1} neurons are primarily responsible for this phenotype and that they act, in part, through projections to the LH. Thus, the pTRN plays an important role in sleep–wake regulation.

Methods

Detailed descriptions of EEG/EMG implantation, recording, and scoring; the sleep deprivation experiment; histology and immunohistochemistry; in situ imaging; stereotaxic viral injection, cannulization, and EEG implantation; action potential silencing; in vivo electrophysiology surgery, recording, and analysis; fiber photometry; chemogenetic experiments; optical cannulas for optogenetics; optical stimulation; electrophysiology; optogenetics analysis; anterograde and CTb tracing; and HCRT/MCH analysis can be found in *SI Appendix, SI Methods*.

Caspase Injection and Video Tracking. ADRB1-Cre or WT littermate mice were injected with 100 to 300 nL of AAV1.hSyn.Flex.taCasp3.TEVp (University of North Carolina [UNC] Vector Core) bilaterally and allowed to recover for 3 to 4 wk before videorecording. Mice were kept in individual cages with free access to food and water. Mice were monitored by infrared camera and tracked by an automatic video tracking system (RRID SCR_014289, Stoelting). Mice were entrained to LD 12:12 for 1 wk, and then locomotor activity was recorded for 4 consecutive days. Mobile times were calculated using the ANY-maze software, and data were averaged using a custom python script. In the ANY-maze software analysis, a mouse was considered immobile if it did not move for 30 consecutive seconds as described previously (19).

For pTRN^{ADRB1} ablation and EEG monitoring, 300 nL of AAV1.hSyn.Flex.taCasp3.TEVp (UNC Vector Core) was injected bilaterally into the pTRN at -4.2 mm (AP), ±0.5 mm (ML), -5.3 mm (DV) and an EEG/EMG head stage was installed as described in the *SI Appendix*. After recording, scoring was done manually using Sirenia Sleep. Then sleep state by hour, total sleep–wake state durations, bout number, bout duration, and transition state probability were analyzed using a custom python script.

Inscopix Implantation. ADRB1-Cre mice were infused unilaterally with 300 nL AAV1.Syn.Flex.jGCaMP7f.WPRE (Addgene #104492-AAV1) into the pTRN using the coordinates described above. One week later, the baseplate surgery was performed. To minimize movement in a deep brain structure, piano wires (California Fine Wire Company, #100165-round 0.002 inches) were attached to the lens with baseplate (Inscopix, #1050-004414) using superglue (Loctite) under a microscope, and jet liquid (Lang Dental, #1406R) was applied to anneal the wires. The wires were attached to extend ∼0.3 mm longer than the lens to stabilize the lens without going through the bottom of the brain.

The day of the surgery, the mouse was anesthetized and wires for the EEG/EMG headset were attached as described previously. To position the EEG headset away from the baseplate, EEG headsets with custom 28-mm EMG lengths (Pinnacle) were used. A hole was drilled above the skull that was slightly larger in diameter than the GRIN lens. Then, using a smaller drill bit (Kopf #8181), small holes were drilled to accommodate the diameter of the GRIN lens + piano wire. Crucially, since the skull hole for the pTRN region is near the fusion of two skull plates near lamda, the holes for the piano wire were drilled diagonally (one rostral and one caudal) offset so that they did not overlap with the skull plate fusion zone to minimize bleeding. Then, the baseplate was slowly lowered on a miniature microscope (Inscopix, nVistsa 2.0) at a rate of 1.0 mm/min until the lens was 1.0 mm above the target area (−5.1 DV from bregma). For the final 1,000 μm, the lens was lowered at a rate of 100 μm/min. The lens was then fixed in place with metabond followed by dental cement. The wires were soldered to the EEG headset, and more dental cement was applied as previously described.

Inscopix Recording. After the lens + baseplate surgery, mice were allowed to recover for at least 3 wk. Mice were recorded in two sessions separated by 1 wk to avoid photobleaching. In each session, the mice were recorded at ZT 3 to 4 and at ZT 13 to 14 at 20 frames per second. The light intensity was calibrated at the start of each recording session to avoid pixel saturation.

Inscopix Imaging Analysis. Imaging data were processed in Mosaic (Inscopix) and python. To correct for lateral motion of the brain relative to the GRIN lens, we used the motion correction function in Mosaic. Regions of interest (ROIs) were then identified using an established algorithm based on principal and independent component analyses (PCA-ICA) followed by visual inspection. The pixel intensities within each ROI were averaged to create a fluorescence time series. For individual neurons, the Z-score was calculated as the difference between the calcium activity at each bin and the averaged calcium activity of the whole recording session, divided by the SD of the whole recording session. Cells were combined across sessions and aligned with sleep stage classification using custom python scripts.

MAPseq Sample Generation. Experiments were conducted as previously described (29, 30). Briefly, 8- to 12-wk-old male mice ($n = 10$) were anesthetized and injected with 225 nL MAPseq Sindbis viral barcode library (3×10^{10} genome copies [GC]/mL, diversity of 2×10^7 unique barcode sequences; Cold Spring Harbor Laboratories) unilaterally into the left pTRN using the above coordinates. The amount of virus for injection was determined by preliminary experiments according to the manufacturer's instructions. The Sindbis virus titer was similar to previous publications that showed that a small fraction of neurons expressed more than one barcode on average. However, as previously discussed (29), neurons expressing greater than one barcode would not change the distribution of projection patterns in the analyzed dataset. Around 44 to 46 h after surgery, mice were rapidly decapitated. Next, the brains were flash frozen in 2-methylbutane (Fisher Scientific) on dry ice. The sections were stored at −80 °C until further processing.

Next, brains were embedded in optimal cutting temperature (O.C.T.) (Fisher Scientific) and sectioned coronally into 200-μm sections on a cryostat (Leica). Sections with the target areas (VLPO, basal forebrain [BF], paraventricular nucleus of the thalamus [PVT], LH, dorsomedial hypothalamus [DMH], VTA, vlPAG, and PZ), negative control area (motor cortex), and the injected source region (pTRN) were mounted on SuperFrost Plus (Fisher Scientific) slides and kept on dry ice. Brain punches of target areas were collected on dry ice with a 500-μm puncher (Electron Microscopy Instruments) that was also chilled on dry ice. To prevent contamination between punches, the puncher was cleaned with 100% ethanol between punches. Samples from each mouse were stored in 1.5-mL microcentrifuge tubes and kept chilled on dry ice until the next stage of processing. Per manufacturer's instruction, each sample was then homogenized in 400 μL of TRIzol (Thermo Fisher), vortexed, then spun down, and then kept on dry ice before shipping to the MAPseq core facility for sequencing and processing (Cold Spring Harbor Laboratories) (29, 30). Barcode extraction and sequencing were completed as previously described (29, 30). Raw barcode reads were subsequently normalized by relative number of spike-in RNAs and put into an N×R matrix with N barcodes found in R regions. Each value in a row represents the number of detected barcodes in that particular region, which corresponds to the projection strength to the region of interest. Matrices were combined for all mice to obtain a single larger matrix. To limit analysis only to cells that project to at least one region, we removed rows that contained all zeros for projection regions.

MAPseq Data Analysis. From a list of barcode reads from the pTRN, negative control, and the eight projection regions, we then created a list of projection neurons, defined as having a read in the pTRN, no reads in the negative control area, and at least one read in the projection region. We binarized the projection motifs so that any sequence read amount greater than 0 was labeled as a 1, and areas without a sequence read were labeled as a zero. Then we performed PCA on the projection motifs and used this binarized dataset to visualize the data using a custom python script.

Single-Cell RT-PCR. At the end of each recording, cytoplasm was aspirated into the patch pipette and then expelled into a PCR tube as described previously (31). The single-cell RT-PCR protocol was designed to detect the presence of mRNAs coding for *Gad1*, *Mch*, *Hcrt*, and *Lhx6*. Reverse transcription and the first

round of PCR amplification were performed with gene-specific multiplex primer using the SuperScript III One-Step RT-PCR kit (12574018, Invitrogen), following the manufacturer's protocol. Second, nested PCR was carried out using Taq DNA polymerase kit (Cat. No. 201207, Qiagen) with nested primers for each gene. Multiplex primers were designed to target two different exons to differentiate genomic DNA from mRNA. The final PCR products were sequenced and verified. Amplification products were visualized via electrophoresis using 1% agarose gel.

Hcrt (forward | reverse):
multiplex, GCCGTCTCTACGAACTGTTGC | CGCTTTCCCAGATCAGGATA
nested, GTCTCTACGAACTGTTGCACG | TTTCCCAGATCAGGATA
Gad1 (forward | reverse):
multiplex, CACAGGTCACCCTCGATTTT | TCTATGCCGCTGAGTTTGTG
nested, TAGCTGGTGAATGGCTGACA | CTTGTAACGAGCAGCCATGA
MCH (forward | reverse):
multiplex, TCCAATGCACTCTTGTTTGG | GAAGGCTACGGATCCTTTCA
nested, TGCTGGCTTTTTCTTTGTTTT | ATCGTTCATGAAACCGCTCT

LHX6 (forward | reverse):
multiplex, CACCTCAAAGCTGATTTGGAC | GGGTTGTTGGCTATTTGGAA
nested, TTTCCCTCTCCTGCTGAGAA | TGAATTAGCCATTGCTGCTG.

Data Availability. Any data generated and/or analyzed in this study are included in the article and/or *SI Appendix*. All custom code data generated in this study are available at https://github.com/johnmichaelwebb/sleep-code.

ACKNOWLEDGMENTS. We thank Dr. Maya Yamazaki and Sherry Tang for genotyping the mice used in these studies. This work was supported by NIH Grants NS099333, NS072360, and NS104782 to L.J.P. and Y.-H.F., and by the William Bowes Neurogenetics Fund to L.J.P. and Y.-H.F.

Author affiliations: [a]Department of Neurology, University of California, San Francisco, CA 94143; [b]Weill Institute for Neurosciences, University of California, San Francisco, CA 94143; [c]Kavli Institute for Fundamental Neuroscience, University of California, San Francisco, CA 94143; and [d]Institute of Human Genetics, University of California, San Francisco, CA 94143

1. S. S. Campbell, I. Tobler, Animal sleep: A review of sleep duration across phylogeny. *Neurosci. Biobehav. Rev.* **8**, 269–300 (1984).
2. T. E. Scammell, E. Arrigoni, J. O. Lipton, Lipton, neural circuitry of wakefulness and sleep. *Neuron* **93**, 747–765 (2017).
3. C. Anaclet *et al.*, The GABAergic parafacial zone is a medullary slow wave sleep-promoting center. *Nat. Neurosci.* **17**, 1217–1224 (2014).
4. J. Lu, M. A. Greco, P. Shiromani, C. B. Saper, Effect of lesions of the ventrolateral preoptic nucleus on NREM and REM sleep. *J. Neurosci.* **20**, 3830–3842 (2000).
5. C. Anaclet *et al.*, Identification and characterization of a sleep-active cell group in the rostral medullary brainstem. *J. Neurosci.* **32**, 17970–17976 (2012).
6. T. C. Chou *et al.*, Critical role of dorsomedial hypothalamic nucleus in a wide range of behavioral circadian rhythms. *J. Neurosci.* **23**, 10691–10702 (2003).
7. K. Liu *et al.*, Corrigendum: Lhx6-positive GABA-releasing neurons of the zona incerta promote sleep. *Nature* **550**, 548 (2017).
8. D. Liu *et al.*, A common hub for sleep and motor control in the substantia nigra. *Science* **367**, 440–445 (2020).
9. S. Ren *et al.*, The paraventricular thalamus is a critical thalamic area for wakefulness. *Science* **362**, 429–434 (2018).
10. T. Tsunematsu *et al.*, Optogenetic manipulation of activity and temporally controlled cell-specific ablation reveal a role for MCH neurons in sleep/wake regulation. *J. Neurosci.* **34**, 6896–6909 (2014).
11. F. Weber *et al.*, Regulation of REM and non-REM sleep by periaqueductal GABAergic neurons. *Nat. Comm.* **9**, 354 (2018).
12. X. Yu *et al.*, GABA and glutamate neurons in the VTA regulate sleep and wakefulness. *Nat. Neurosci.* **22**, 106–119 (2019).
13. Z. Zhang *et al.*, An excitatory circuit in the perioculomotor midbrain for non-REM sleep control. *Cell* **177**, 1293–1307.e16 (2019).
14. N. P. Pedersen *et al.*, Supramammillary glutamate neurons are a key node of the arousal system. *Nat. Commun.* **8**, 1405 (2017).
15. L. de Lecea *et al.*, The hypocretins: Hypothalamus-specific peptides with neuroexcitatory activity. *Proc. Natl. Acad. Sci. U.S.A.* **95**, 322–327 (1998).
16. R. M. Chemelli *et al.*, Narcolepsy in orexin knockout mice: Molecular genetics of sleep regulation. *Cell* **98**, 437–451 (1999).
17. L. Lin *et al.*, The sleep disorder canine narcolepsy is caused by a mutation in the hypocretin (orexin) receptor 2 gene. *Cell* **98**, 365–376 (1999).
18. G. Shi *et al.*, A rare mutation of β1-adrenergic receptor affects sleep/wake behaviors. *Neuron* **103**, 1044–1055.e7 (2019).
19. Y. He *et al.*, The transcriptional repressor DEC2 regulates sleep length in mammals. *Science* **325**, 866–870 (2009).
20. L. Xing *et al.*, Mutant neuropeptide S receptor reduces sleep duration with preserved memory consolidation. *Sci. Transl. Med.* **11**, eaax2014 (2019).
21. G. Shi *et al.*, Mutations in metabotropic glutamate receptor 1 contribute to natural short sleep trait. *Curr. Biol.* **31**, 13–24.e4 (2021).
22. U. Rub *et al.*, Damage to the reticulotegmental nucleus of the pons in spinocerebellar ataxia type 1, 2, and 3. *Neurology* **63**, 1258–1263 (2004).
23. C. J. Hung, D. Ono, T. S. Kilduff, A. Yamanaka, Dual orexin and MCH neuron-ablated mice display severe sleep attacks and cataplexy. *eLife* **9**, e54275 (2020).
24. S.-R. Yang *et al.*, The rostromedial tegmental nucleus is essential for non-rapid eye movement sleep. *PLoS Biol.* **16**, e2002909 (2018).
25. M. Xu *et al.*, Basal forebrain circuit for sleep-wake control. *Nat. Neurosci.* **18**, 1641–1647 (2015).
26. W. Peng *et al.*, Regulation of sleep homeostasis mediator adenosine by basal forebrain glutamatergic neurons. *Science* **369**, eabb0556 (2020).
27. A. Venner, C. Anaclet, R. Y. Broadhurst, C. B. Saper, P. M. Fuller, A novel population of wake-promoting GABAergic neurons in the ventral lateral hypothalamus. *Curr. Biol.* **26**, 2137–2143 (2016).
28. A. Venner *et al.*, An inhibitory lateral hypothalamic-preoptic circuit mediates rapid arousals from sleep. *Curr. Biol.* **29**, 4155–4168.e5 (2019).
29. J. M. Kebschull *et al.*, High-throughput mapping of single-neuron projections by sequencing of barcoded RNA. *Neuron* **91**, 975–987 (2016).
30. M. M. Gergues *et al.*, Circuit and molecular architecture of a ventral hippocampal network. *Nat. Neurosci.* **23**, 1444–1452 (2020).
31. B. Lambolez, E. Audinat, P. Bochet, F. Crépel, J. Rossier, AMPA receptor subunits expressed by single Purkinje cells. *Neuron* **9**, 247–258 (1992).